A Multiscale Computational Study of Cellulose Acetate-Water Miscibility: Insights from Molecularly Informed Field-Theoretic Modeling

My V. T. Nguyen,[†,‡] Nicholas Sherck,[†,¶] Stephan Köhler,[§] Eduard Schreiner,[§] Rohini Gupta,[‖] Glenn H. Fredrickson,[*,‡,⊥,#] and M. Scott Shell[*,‡]

†*Equal contribution*

‡*Department of Chemical Engineering, University of California, Santa Barbara, California, 93106, United States*

¶*BASF Corporation, Iselin, New Jersey 08830, United States*

§*BASF SE, Ludwigshafen am Rhein 67056, Germany*

‖*California Research Alliance (CARA) by BASF, Berkeley, California 94720, United States*

⊥*Materials Research Laboratory, University of California, Santa Barbara, California, 93106, United States*

#*Department of Materials, University of California, Santa Barbara, California, 93106, United States*

E-mail: ghf@ucsb.edu; shell@ucsb.edu

For Table of Contents use only

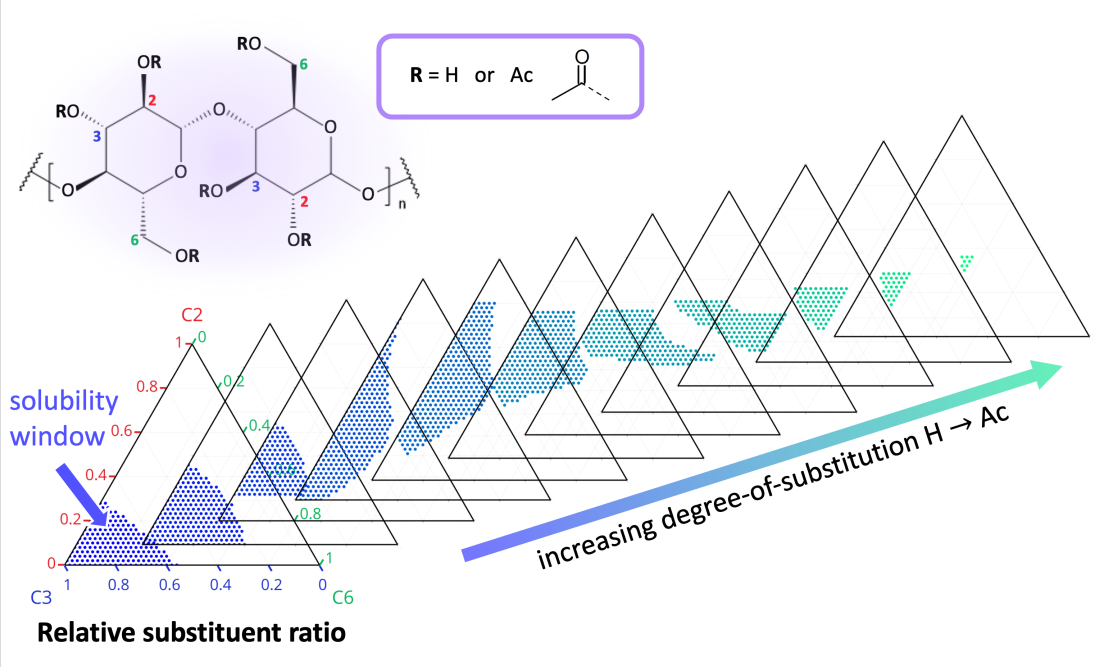

Abstract

Cellulose acetate (CA), a prominent water-soluble derivative of cellulose, is a promising biodegradable ingredient that has applications in films, membranes, fibers, drug delivery, and more. In this work, we present a molecularly informed field-theoretic model for CA to explore its phase behavior in aqueous solutions. By integrating atomistic details into large-scale field-theoretic simulations via the relative entropy coarse-graining framework, our approach enables efficient calculations of CA's miscibility window as a function of the degree-of-substitution (DS) of cellulose hydroxyl groups with acetate side chains. This allows us to capture the intricate phase behavior of CA, particularly its unique miscibility at intermediate substitution, without relying on experimental input. Additionally, the model directly probes CA solution behavior specific to the relative DS at C2, C3, and C6 alcohol sites, providing insights for the rational design of water-soluble CA for diverse applications. This work demonstrates a promising integration of molecularly informed field-theories, complementing wet-lab experimentation, for engineering the next-generation polymeric materials with precisely tailored properties.

Keywords: cellulose, molecular modeling, bottom-up coarse-graining, field theory

1 Introduction

Carbohydrates are appealing from a sustainability perspective as they are bio-sourced and are often biodegradable.[1] For example, cellulose has great potential as a bio-sustainable additive in formulations. However cellulose itself is insoluble in water (and many other solvents) due to its strong tendency to crystallize resulting form numerous inter- and intra-chain hydrogen bonds and hydrophobic forces limiting its direct utility in aqueous formulations.[2,3] To improve cellulose's aqueous solubility and tailor material properties the alcohols are functionalized; in particular, cellulose acetate (CA) is one of the most prevalent cellulose derivatives finding widespread use in films, membranes, fibers, and drug delivery, among others.[4] The literature contains numerous studies demonstrating that tuning the degree-of-substitution (DS) of the alcohols (yellow highlights in Fig. 1) with acetate, modulates cellulose solubility in a variety of solvents but in particular in water.[5,6] While the DS regulates solubility, it also greatly influences the rate of biodegradation with lower DS chains degrading faster.[7,8]

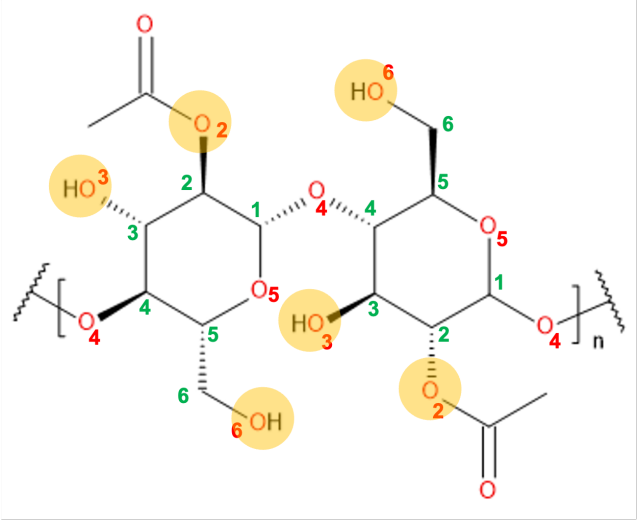

Figure 1: Representative cellulose structure consisting of two glucose monomers, each with one alcohol at the C2 position substituted with an acetate group (DS=1). The yellow highlights denote the oxygens in the alcohols available for acetylation, while the green and red numbers denote the carbon and oxygen numberings, respectively.

Broadly speaking, the literature suggests there are two routes to achieve partially acetylated CA. The first and oldest technique is a two-step process that involves first completely acetylating the cellulose (DS $\sim$ 3) followed by partial deacetylation under acidic or basic conditions.[9–11] This is a harsh process and leads to degradation of the acetal linkages along the cellulose backbone. More recent developments have aimed at one-step strategies that are less harsh and less involved, such as acetylation in an ionic liquid.[4] A critical difference between the one- and two-step synthesis techniques is that they typically yield different ratios of substitution between the three alcohol sites. Albeit, in the two-step method during the deacetylation step, reacetylation is believed to occur, which obscures direct measurement of alcohol reactivities through quantification of the relative DS substitutions.[12] In the one-step method the C6 position is preferably acetylated with relative ratios for C6:C3:C2 of 14.1:3.7:1.0, respectively (at a total DS of 0.63).[4] Kamide *et al.* have observed that one-step protocols indeed lead to a greater fraction of C6 substitution relative to the two-step method; however, they didn't observe a region of water solubility for CA produced by a one-step protocol.[10] Since Kamide *et al.* observed a more distributed DS among the alcohol sites in the

two-step method, they concluded that acetylation at both the C2 and C3 positions are more important for water solubility than for C6 alone.

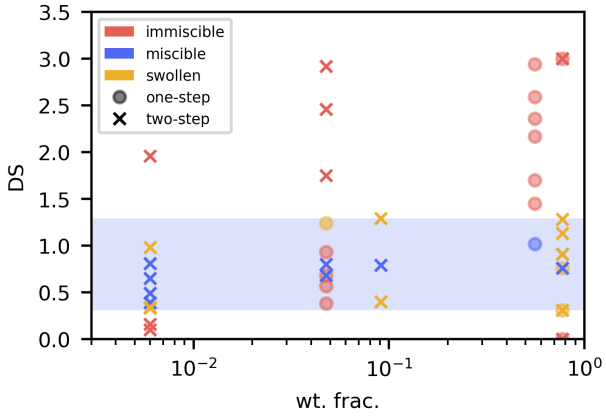

Figure 2: Cellulose acetate solubility data compiled from the literature. Circle and cross symbols denote one-step and two-step routes, respectively. Colors denote immiscible (red), swollen/partially soluble cellulose acetate (yellow), and miscible (blue). Shaded blue region approximately indicates miscible or swollen cellulose acetate from the *two-step* synthesis route.

Data on CA solubility in water, compiled from various literature sources,[4,6,10,12–18] indicates a loosely defined region of solubility, spanning DS values between 0.3 to 1.3 (Fig. 2). Unfortunately, many of the literature sources do not clearly define their protocols for assessing "solubility". There are several factors that can change the solubility in addition to the DS and synthesis method (one- or two-step): (1) CA molecular weight and polydispersity, (2) temperature, (3) method to mix and assess if soluble, and (4) the relative ratios of acetylation at the three alcohol sites, which is dependent on the exact reaction conditions and particular protocol, either one- or two-step. When considering all available data (Fig. 2, both circle and cross symbols), there is uncertainty around where CA and water are miscible, with both insoluble and soluble datasets overlapping; considering only two-step data a clear DS region appears for which CA is either soluble or swollen, shown in the shaded blue region of Fig. 2. Overall, missing is a detailed investigation into systematically mapping out the DS-composition phase diagram of CA-water mixtures. Further detailed studies on both the experimental and simulation fronts are needed to develop a better picture of

the factors influencing CA solubility while establishing a more comprehensive and accurate phase diagram.

In this work, we develop a molecularly informed field-theoretic model in a proof-of-concept demonstration of this multiscale approach for studying polysaccharides and predicting their solubility. Specifically, we use the workflow to systematically study the impact of DS on the aqueous phase behavior of CA at room temperature. The construction of the CA model expands our earlier work in developing and applying molecularly informed field theories to several classes of (macro)molecules and formulations thereof.[19–23] Leveraging the computational efficiency of the field theory in enabling direct and rigorous calculations of the free energy, we determine the phase boundary, which not only sheds light on how acetylation pattern and DS influence the miscibility of CA but also precisely identifies CA compositions that lead to miscible samples. More importantly, this work delineates the role of distinct acetylation sites and underscores their significance in CA's solubility. Such insights are vital for guiding the design and synthesis of water-soluble CA with targeted properties for a wide range of applications and provides a computational platform for in silico screening of CA formulations.

2 Computational details and methods

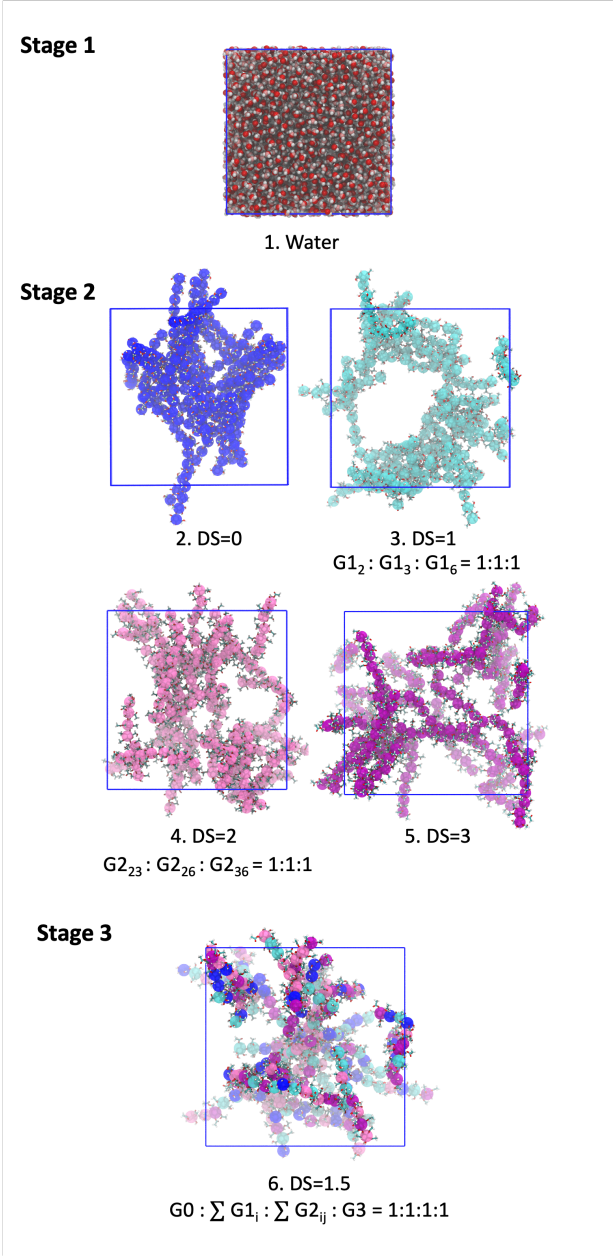

Figure 3: All-atom simulations used to derive coarse-grained interaction parameters via the relative entropy coarse-graining framework. In simulations 2-6, we overlay the coarse-grained bead types corresponding to the repeating units defined in Fig. 4; water is not shown for clarity. We denote underneath simulations 3, 4, and 6 the relative ratio of different glucose monomers in the simulation. Gx denotes a glucose repeating unit with x alcohol sites being substituted for acetate. For G1 and G2 monomers, the subscripts denote the acetylated alcohol sites (2, 3, or 6). Simulations details are provided in Table S1

2.1 All-atom simulations

We parameterize the pair-wise and bonded interactions for the coarse-grained (CG) model via three stages based on six reference all-atom (AA) simulations as presented in Fig. 3. We use the CHARMM carbohydrates atomistic force field[24] along with the Optimal Point Charge (OPC) 4-point water model;[25] any missing dihedral parameters of the acetate group on the primary alcohol are taken from the CHARMM General FF (CGenFF).

The first simulation is a pure water box with an average side length of 4.7 nm. For simulations 2-6 (refer to Fig. 3), we perform molecular dynamics simulations on cellulose oligomers, each consisting of 8 repeat units, with varying DS. During these simulations, we randomly select alcohols along the backbone of each cellulose chain to acetylate, while ensuring that the acetate groups are distributed equally among the three alcohol sites whenever applicable (simulations 3, 4, and 6). In simulations 2-5, we additionally constrain the DS of all repeating units to be the same. In contrast, in simulation 6, we consider mixed DS values (DS=0, 1, 2, or 3) for the repeating units and ensure there is an equal number of monomers for each DS value.

We conduct reference AA simulations with the OpenMM simulation package.[26] A 1 nm cutoff is employed for the direct space non-bonded interactions and we use the Particle Mesh Ewald method to compute long range Coulomb and Lennard-Jones interactions (LJPME method in OpenMM). In addition, we constrain the length of all bonds that involve a hydrogen atom and employ a time step of $dt = 0.002$ ps. The temperature is set to 298.15 K using the Langevin thermostat with a friction coefficient of 5 ps^{-1}, while the pressure is set to 1 atm using a Monte Carlo barostat with an update frequency of $1/(25\ dt)$. We initialize configurations using the CHARMM builder feature inside of VMD 1.9.3[27] (http://www.ks.uiuc.edu/Research/vmd/) and solvate the chains with water using Packmol.[28] Details of the system sizes are provided in Table S1.

2.2 Bottom-up coarse-graining

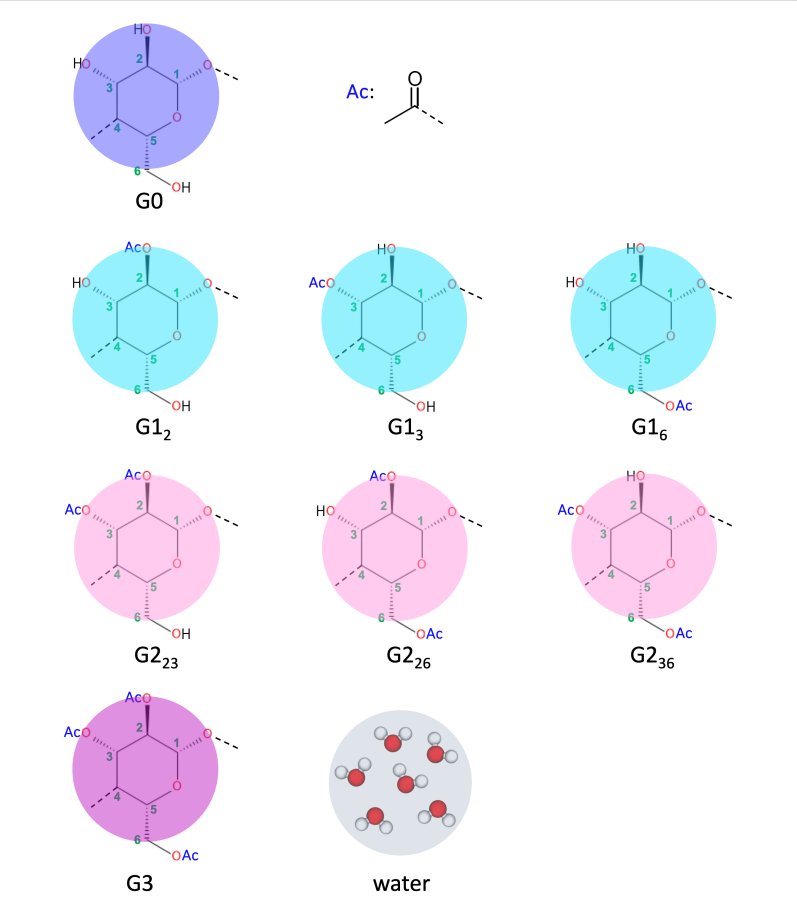

Figure 4: Schematic of the 9 coarse-grained bead types for unsubstituted (G0), partially substituted (G1$_i$ and G2$_{ij}$), fully substituted (G3) glucose monomers, and CG water composed of, on average, 6 atomistic water molecules. Subscripts i, j denote the alcohol site that acetylation occurs; $i = 2, 3, 6$ corresponds to sites C2, C3, and C6, respectively.

Although we provide details about the choice of CG potential in previous publications,[20–23,29] we briefly discuss them here. After performing AA simulations as described in the previous section, we use relative entropy coarse-graining[30] with these as references to parameterize CG interaction potentials that are amenable to exact analytical conversion to a field theory. In the CG model, bonded interactions in the cellulose molecule are described using a harmonic bond potential:

$$\beta U_{b,\alpha\gamma}(r) = \frac{3}{2b_{\alpha\gamma}^2} r^2, \tag{1}$$

where $\beta = 1/k_BT$, r is the distance between two bonded beads, and $b_{\alpha\gamma}$ is the root-mean-square length of a bond between bead species α and γ. For simplicity, we assume one bond length for all monomer pairs, $b_{\alpha\gamma} \equiv b$. The excluded volume interactions between all site pairs, including bonded pairs, are described by pairwise terms involving repulsive Gaussian potentials:

$$\beta U_{ev,\alpha\gamma} = v_{\alpha\gamma} e^{-r^2/2(a_\alpha^2 + a_\gamma^2)} \tag{2}$$

where $v_{\alpha\gamma}$ is the excluded volume strength between bead species α and γ, and a_α is the Gaussian regularization length of bead species α. This choice of regularized, soft potentials is physically motivated by the desire to retain long-length-scale physics while coarse-graining over sharp, short-length-scale features. The Gaussian form of the potential also has an analytical functional inverse, which facilitates conversion of the CG model into field-theoretic form.[31]

We translate AA reference trajectories for coarse-graining by mapping center-of-mass coordinates of groups of atoms in the AA representation to CG sites as shown in Fig. 4. Specifically, we map each repeating glucose unit of cellulose into a single neutral bead. We use eight bead types to represent the different chemistries of the glucose monomers based on the DS and location of acetate group. There are three monomer types with DS = 1, $G1_2$, $G1_3$, and $G1_6$, corresponding to acetylation at C2, C3, and C6 sites, respectively. Similarly, $G2_{23}$, $G2_{26}$, and $G2_{36}$ represent monomers of DS = 2 with sites C2 and C3, C2 and C6, and C3 and C6 acetylated, respectively.

In the CG model, we represent several atomistic water molecules by a single neutral bead. This is inspired by the challenge of studying long length and time-scale phenomena in explicit-solvent simulations, even with the reduced resolution in CG simulations. It also aims to ensure uniform bead sizes across all CG bead types. Here, we use the k-means clustering algorithm[32–34] to identify clusters of water molecules in each reference trajectory

frame by minimizing the within-cluster sum of variances of coordinates. While the number of molecules in each cluster cannot be directly controlled, the total number of clusters, k, or the total number of CG water molecules, determines the average number of water molecules in each cluster. We specify k such that the average cluster size is 6, i.e., each CG bead of water represents, on average, 6 atomistic water molecules. The Scikit-learn library[35] is employed to carry out the clustering process. We set the maximum number of iterations to 500 and repeat the k-means algorithm with different centroid seeds 20 times. We ensure that these parameters are sufficiently large by monitoring the convergence of the average number of water molecules per cluster and the average cluster sphericity index (Fig. S1). The latter is a metric used to evaluate the shape of a cluster of atomistic water molecules. We fix the Gaussian regularization range, a_α, of each bead species to approximately the cube root of its molecular volume, estimated from AA simulations. Since with this approach the molecular volume of all CG bead types are comparable, we set $a_\alpha = 0.6$ nm for all species.

We derive CG parameters in three successive stages; once parameters are determined, they are fixed in subsequent steps. In the first stage, we determine the water-water repulsion v_{ww} from pure water AA simulation to reproduce the compressibility of OPC water, $\kappa_T \sim 4.51 \times 10^{-10}$ Pa^{-1}. This determines the CG pressure of $P_{CG} = 285.99\ k_BT/nm^3$ that we use in the subsequent coarse-graining stages.

In the second stage, we parameterize the excluded volume interactions between glucose monomers of same DS values (DS = 0, 1, 2, and 3) and their cross interactions with water via 4 reference simulations, each composed of uniformly substituted cellulose molecules in water (simulations 2-5 in Fig. 3). The parameters derived in this step are $v_{G0\,G0}$, $v_{G1_i\,G1_j}$, $v_{G2_{ij}\,G2_{kl}}$, $v_{G3\,G3}$, $v_{G0\,w}$, $v_{G1_i\,w}$, $v_{G2_{ij}\,w}$, and $v_{G3\,w}$, where the subscripts i, j, k, and l denote the alcohol sites that are acetylated ($i, j, k, l \in [2, 3, 6]$).

In stage three, we derive the remaining cross-interactions among the glucose monomers ($v_{G0\,G1_i}$, $v_{G0\,G2_{ij}}$, $v_{G0\,G3}$, $v_{G1_i\,G2_{jk}}$, $v_{G1_i\,G3}$, and $v_{G2_{ij}\,G3}$) along with one universal bond length, b, for all monomer types from a simulation at DS = 1.5 (simulation 6 in Fig. 3) where

monomers are randomly substituted while maintaining the ratio G0 : $\sum_i$G1$_i$: $\sum_{ij}$G2$_{ij}$: G3 as 1:1:1:1 and acetate groups are distributed equally to three alcohol sites. ~~We tabulate the parameters in Tables~~ S2 ~~and~~ S3.

We perform each of the above coarse-graining steps in three independent trials to evaluate the parameter uncertainty. Specifically, as presented in Fig. S2, 43 out of 45 excluded volume parameters, $v_{\alpha\gamma}$, exhibit a standard deviation less than 0.02 k_BT. Notably, the parameter variance is inversely correlated with the diagonal terms of the Hessian of S_{rel} (Fig.S3); this is expected since the Hessian is also the Fisher information, which inversely corresponds to the variance of the estimated parameter.[19] Further analysis, discussed later, suggests that the CG parameter uncertainty has minimal influence on our investigation of CA miscibility. Therefore, we use one set of CG parameters from one of the three trials for miscibility prediction from here on, and we tabulate these parameters in Tables S2 and S3.

2.3 Coarse-grained molecular dynamics (CGMD)

CGMD simulations are conducted using a Langevin Dynamics integrator. The Langevin relaxation time τ_{CG} is taken as the unit of time. Due to the soft nature of the CG interactions and bonds, large time steps of 0.02 τ_{CG} are feasible. During the relative entropy minimization step, CG configurations are sampled from short trial CGMD which we run for 2.5×10^6 time steps, or 5×10^4 τ_{CG}. We employ a cutoff of 3 nm ($5 \times a_\alpha$) for the non-bonded pair-wise interactions, sufficient for the Gaussian excluded volume interactions to become negligible.

2.4 Phase diagram calculation with the field theory

The CG model defined in Section 2.2 can be exactly represented in a field theoretic form via the Hubbard-Stratonovich-Edwards transformation.[31,36,37] This transformation decouples the non-bonded pair interactions such that particles interact only via the bonded potential and with auxiliary fields introduced by the transform. The result is a partition function in

terms of integrals over field configurations instead of particle coordinates:

$$\mathcal{Z} = \int d\boldsymbol{r}^n e^{-\beta U(\boldsymbol{r}^n)} \rightarrow \int \mathcal{D}w e^{-H[\boldsymbol{w}]}, \tag{3}$$

where H is an effective Hamiltonian describing the statistical weight of the auxiliary field configuration $w(\boldsymbol{r})$, and is described in detail elsewhere.[31,37] It should be emphasized that $\boldsymbol{w}$ represents a set of auxiliary fields that is sufficient to decouple all pairwise interactions of the functional forms defined in Section 2.2.

To identify the two-phase boundary for CA aqueous mixtures, we employ the Gibbs ensemble method and invoke the mean-field approximation for the free energy and chemical potential calculations. In the mean-field approximation, the canonical partition function takes the form:

$$\mathcal{Z} \approx e^{-H[w^*]} \equiv e^{-H^*} \tag{4}$$

where w^* is the saddle-point value of each auxiliary field, representing the dominant field configuration contributing to the partition function, and H^* is the effective Hamiltonian, equal to the dimensionless Helmholtz free energy βA in the mean-field approximation. This approximation reduces computational cost significantly compared to sampling w field configurations. A detailed discussion of calculating phase diagrams using the Gibbs ensemble can be found in our previous publication.[21]

3 Results and Discussion

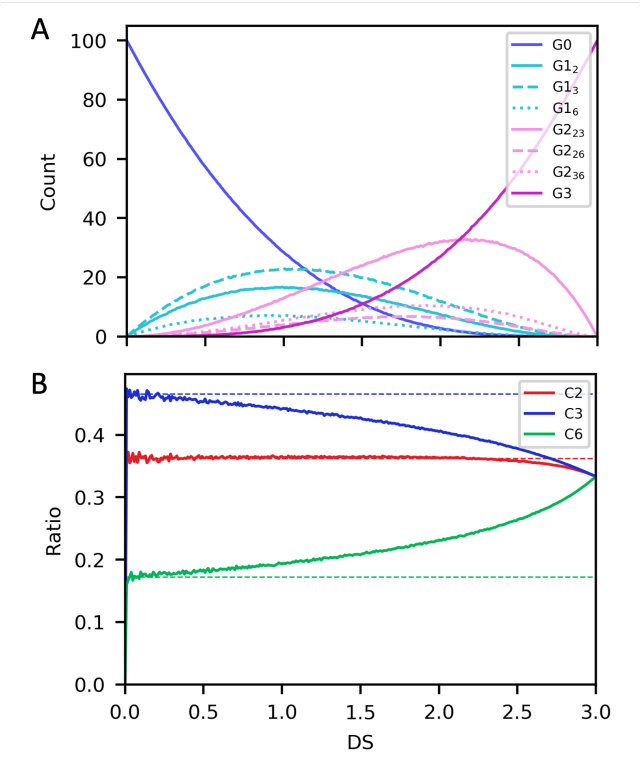

Figure 5: (A) Count of 8 coarse-grained bead types comprising CA at varying DS for cellulose chains of length $N = 100$ and $r_{set} = 0.36 : 0.47 : 0.17$. r_{set} represents the relative likelihood of substitution at the C2, C3, and C6 sites (see main text for its definition). The count is averaged over 1000 sequence generations at each DS value to obtain the most representative sequence. (B) Relative substituent ratios at C2, C3, and C6 corresponding to the representative sequences in (A). Dashed lines represent r_{set}.

At zero and full substitution (DS = 0 and 3), cellulose is composed solely of the unsubstituted and fully substituted monomers, G0 and G3, respectively. For intermediate DS values, we determine the monomer composition of cellulose by assigning acetate independently to three alcohol sites (C2, C3, and C6) based on the ratios C2:C3:C6 $\equiv r_{set}$. At a given DS value, we restrict the number of substitutions to DS $\times N$, where N is the degree of polymerization. This process is repeated 1000 fold to obtain an average monomer composition at each DS value. An example of the resulting monomer counts averaged over the generated sequences

at DS values ranging from 0 to 3 is shown in Fig. 5A. In this specific example, we set the acetylation ratio $r_{set} = 0.36 : 0.47 : 0.17$, which aligns with the average relative substituent composition reported for water-soluble CA samples by Buchanan *et al.* (1991).[18]

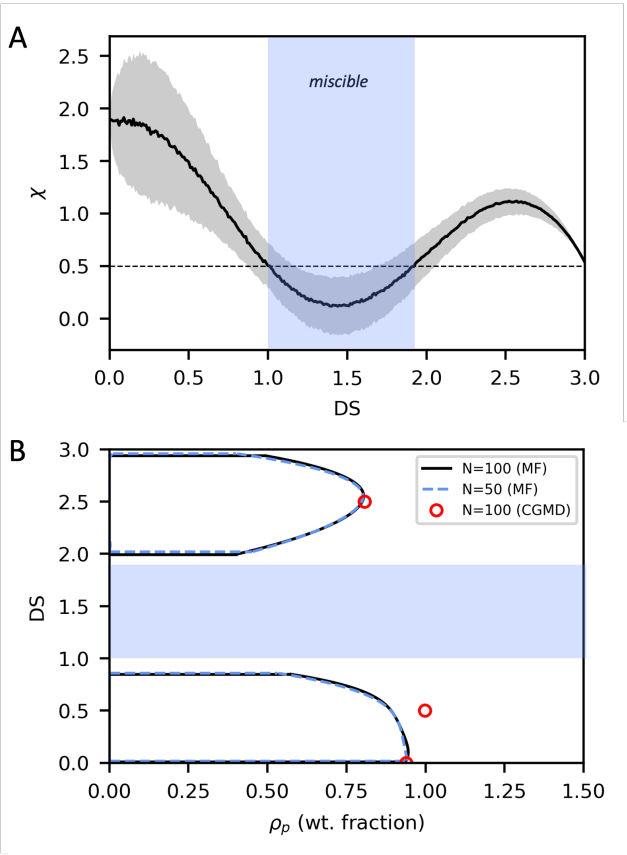

Figure 6: (A) Effective χ of CA as a function of DS for the representative sequences in Fig. 5. Shaded gray area denotes the standard deviation of χ over 1000 sequence generations. A miscibility window, denoted by the shaded blue region, is predicted for intermediate DS values in which $\chi < 0.5$. The miscibility window is consistent with results in (B), phase diagrams calculated using the Gibbs ensemble method for $N = 50$ and 100. Open red symbols indicate compositions of the dense phase calculated from CGMD for $N = 100$. Again, the shaded blue region is the miscible region from (A).

We note that for DS > 1.0, the design space defined by the ratio C2:C3:C6 becomes more constrained as DS increases (illustrated by the shaded region in Fig. S4). For instance, at DS=3, it is not feasible to have a monomer composition with all substitutions at the C2 alcohol and none at C3 or C6 alcohols (C2:C3:C6 = 1:0:0). In this case, all three sites need to be substituted, such that only the ratio C2:C3:C6 = 1:1:1 is possible. This illustrates that

when we set a specific C2:C3:C6 (r_{set}) ratio during acetate assignment, we are not directly determining the resulting ratio C2:C3:C6 in the generated cellulose sequence. Consequently, by defining the ratio C2:C3:C6 during acetate assignment, we influence the probability of substitutions at the respective sites, but the actual relative substituent ratio, r_{actual}, is also determined by the design space imposed by the chosen DS value. Figure 5B presents the actual substituent ratio at the three alcohol sites, showing that r_{actual} is not equal to r_{set}. Instead, r_{actual} varies with DS and approaches 1:1:1 at DS=3.

We first characterize the propensity for macrophase separation as a function of DS by an effective Flory-Huggins parameter, χ.[38,39] The binary interaction χ approximates the overall affinity of CA for the aqueous solvent, where a higher value of χ indicates a greater tendency towards phase separation. In this work, χ is defined as:

$$\chi = v_{ref}\left(\rho_w^*\rho_p^* U_{p\,w} - \frac{1}{2}(\rho_p^{*2}U_{p\,p} + \rho_w^{*2}U_{w\,w})\right), \tag{5}$$

where subscripts p and w denote molecule species for cellulose and water, respectively, and the reference volume v_{ref} is taken to be the molecular volume of water, $v_{ref} = (\rho_w^*)^{-1}$. The neat density of *molecule* species i, ρ_i^*, is estimated from a mean-field approximation (detailed in the supporting information of ref. 21) as follows:

$$\rho_i^* = \frac{-1 + \sqrt{1 + 2U_{ii}P_{CG}}}{U_{ii}}, \tag{6}$$

where P_{CG} is the CG pressure discussed in Section 2.2. Eq. 5 and 6 involve the excluded volume parameter U_{ij} between *molecules* i and j, which is defined by summations over bead and molecule species:

$$U_{ij} = \sum_{\alpha,\gamma\,\in[w,Gx]}\ \sum_{i,j\,\in[w,Gx]} u_{\alpha\,\gamma} f_{i,\alpha} f_{j,\gamma} N_i N_j, \tag{7}$$

where $u_{\alpha\gamma}$ is the integrated value of the excluded volume interaction $\beta U_{ev,\alpha\gamma}$ between *beads* α and γ, i.e., $u_{\alpha\gamma} = v_{\alpha\gamma}(2\pi(a_\alpha^2 + a_\gamma^2))^{3/2}$. The number fraction of bead α on chain i is denoted

as $f_{i,\alpha}$, and the chain lengths of water and cellulose are $N_w = 1$ and $N_p = N$, respectively. According to this definition, the excluded volume strength between water molecules is the same in both the bead-basis and molecule-basis definitions, i.e., $U_{ww} = u_{ww}$.

In our definition of χ, only the relative composition of monomer types is important and χ is independent of chain length and patterning. The latter assumes that the specific arrangement or pattern of the monomers within the cellulose sequence does not influence its value; this is consistent with the mean-field approximation of Eq. 4. After obtaining χ for all the generated sequences at a particular DS, we calculate the average of these values to arrive at a representative or typical χ value for the given DS. We plot the average χ as a function of DS for $r_{set} = 0.36 : 0.47 : 0.17$ in Fig. 6A. As a first approximation, phase separation occurs at $\chi \gtrsim 0.5$,[40] suggesting that the our model predicts CA is insoluble for DS $\lesssim 1$ and $\gtrsim 2$.

Fig. 6B shows the phase diagram for two different chain lengths, $N = 100$ and $N = 50$, calculated directly in the mean-field limit using the Gibbs ensemble approach based on the average monomer compositions (Fig. 5A) at $r_{set} = 0.36 : 0.47 : 0.17$. The miscibility window is observed at intermediate DS values from 1.0 to 2.0, in line with the predictions made by the effective χ values. In contrast to the χ analysis, the binodal calculation rigorously accounts for composition dependence which provides the specific composition and DS at which CA becomes miscible. The agreement between the binodal phase diagram and the effective χ values suggests the viability of using the approximate effective χ as a proxy to quickly determine phase separation in CA solutions. We repeat the χ calculation for the other two CG parameter sets (resulting from multiple independent coarse-graining trials as previously mentioned in Section 2.2) and find that the three miscibility windows, defined by $\chi < 0.5$, are indistinguishable. This further confirms that uncertainty in CG parameters has a minimal effect on miscibility predictions (Fig. S5).

Additionally, we find that the dense branch of the 2-phase boundary is insensitive to the chain length N (Fig. 6B), indicating that the results presented here have approached the

long-chain limit. This suggests that results obtained at $N = 100$ can be reasonably extrapolated to larger molecular weights used in experiments. Additionally, the close agreement between the CA composition in the dense phase as predicted by the mean-field approximation and CGMD simulations at DS values of 0, 0.5, and 2.5 further suggests that the mean-field approximation provides a reasonable description of phase separation in this system.

More importantly, we are able to qualitatively reproduce the miscibility window at intermediate DS values that has been previously observed for DS $\sim 0.3 - 1.3$ by various experimental studies[12,16,18] for CA as summarized in Fig. 2. The emergence of the miscible region with increasing DS in CA has been attributed to the disruption of the hydrogen bonding network within the cellulose matrix.[4,12] Intra-molecular hydrogen bonding contributes to the amphiphilic nature of cellulose, which helps to maintain cellulose's crystallinity, while inter-molecular hydrogen bonding maintains the close packing of cellulose chains.[3,41,42] As the AA simulations suggest, when DS increases more alcohol groups are replaced by acetate groups, leading to a disruption of the hydrogen bonding network between cellulose molecules and inducing a conformational change. Consequently, the unsubstituted alcohol groups become more exposed to water, the hydrophobic plane of the cellulose backbone is disrupted with neighboring rings no longer lying parallel, and the nonuniform acetylation patterning introduces disorder that further inhibits crystallization. When a significant portion of the alcohol groups are substituted by acetate at high DS, the chain becomes less hydrophilic because acetate groups cannot form as many hydrogen bonds with water as the alcohol groups. Consequently, this leads to the reappearance of the immiscibility window at high DS values.

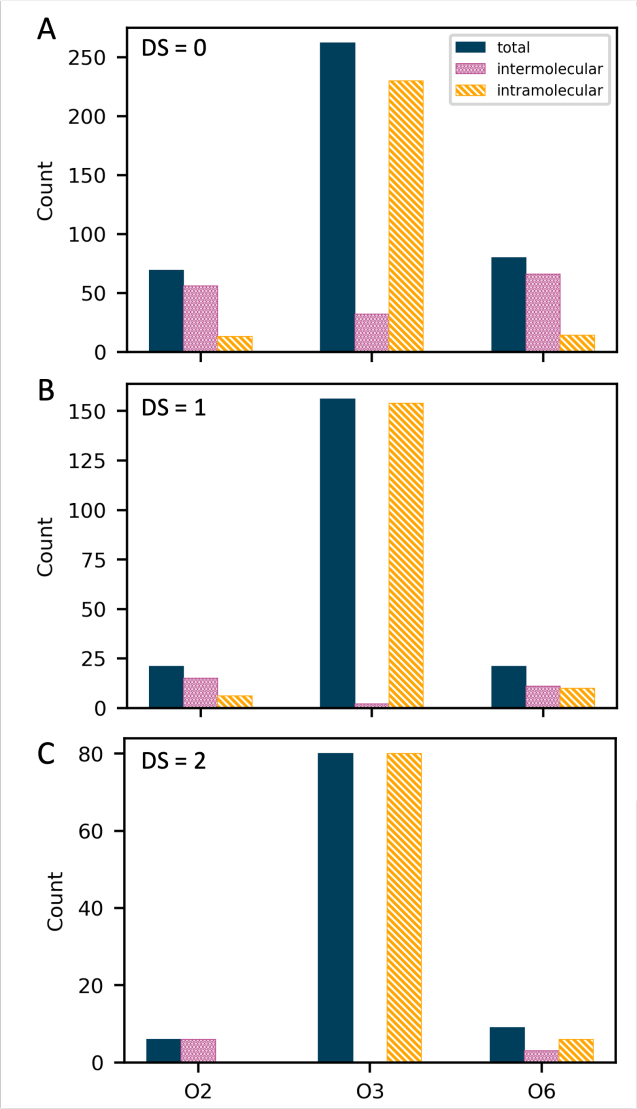

Figure 7: Number of total, inter-, and intra-molecular hydrogen bonds between monomers of cellulose that involve oxygens O2, O3, and O6 of the alcohol groups at the C2, C3, and C6 sites, respectively, calculated from AA simulations of 8-mers at (A) DS=0, (B) DS=1, and (C) DS=2, corresponding to simulations 2, 3, and 4 in Fig. 3. In each simulation, all monomers have the same DS value and acetate groups are equally distributed to all sites. Number of hydrogen bonds by atom pairs are summarized in Fig. S7.

To understand the origin of the miscibility window predicted by the model at low DS values, we compute effective χ values for homopolymers composed of each of the 8 monomer types. This provides a simple metric to assess the individual monomer's preference for hydration. Notably, Fig. S6 illustrates that the $G1_3$ monomer has the lowest effective χ value, below 0.5, in comparison to the other monomers. This finding suggests that the

emergence of miscibility, as predicted by the model at intermediate DS values, stems from the increase in hydrophilicity associated with the increase in the number of $G1_3$ monomer relative to the more hydrophobic monomers like G0 and $G1_2$. Notably, this observation aligns with experimental observations that selectively acetylating C3 results in water-soluble CA because it disrupts hydrogen bonding involving the alcohol group at the C3 position, which plays a crucial role in maintaining the crystalline structure of cellulose.[4,12]

We verify this hypothesis by calculating the number of hydrogen bonds between all monomers from reference AA simulations of 8-mers, where all monomers have the same DS value and substituents are equally distributed to all alcohol sites at DS values 0, 1, and 2 (simulations 2, 3, and 4 in Fig. 3, respectively). As depicted in Fig. 7, there are more total hydrogen bonds involving the oxygen at the C3 alcohol group (O3) compared to those involving the alcohols at either the C2 or the C6 positions (O2 and O6, respectively).

Moreover, as the alcohols are substituted the relative orientation between the glucopyranose rings shifts further from the expected 180° antiparallel structuring found in crystalline cellulose[43] to having significant populations of conformations at offsets nearer 130°-140°, see SI Fig. S8 and Fig. S9. We do not observe perfect antiparallel structuring for virgin cellulose in the distributions from our simulations as we do not use any special treatment to initialize the chains and they are relatively short oligomers; instead, the virgin cellulose oligomers have a bimodal glucopyranose ring distribution with nearly even populations existing near 160° and 140° for DS=0. Notably, the conformational change is greatest when only acetylating the C3 position ($G1_3$ is the most hydrophilic monomer) nearly erasing any signature of the population of conformations near 160°, while both $G1_2$ and $G1_6$ retain strong signatures of the biomodal distribution in ring conformations like the unacetylated cellulose. This conformational change is tied to the addition of the large steric group at the C3 position, which also disrupts the intrachain O3-O5 hydrogen bond between consecutive cellulose monomers that otherwise remain prevalent in the $G1_2$ and $G1_6$ monomers, refer to SI Fig. S9.

The ability of the CG model to qualitatively capture these effects of substitution on solu-

bility underscores the model's capability to predict highly nontrivial phase behavior without any experimental input. Nevertheless, the use of this multiscale workflow enables us to interrogate macroscopic phase behavior while allowing for probing the subtle interplay of inter- and intra-molecular forces underpinning the macroscopic behavior of partially acetylated cellulose (in-)solubility. In fact, cellulose and its derivatives' (in-)solubility in water remains an area of intense research.[44–46]

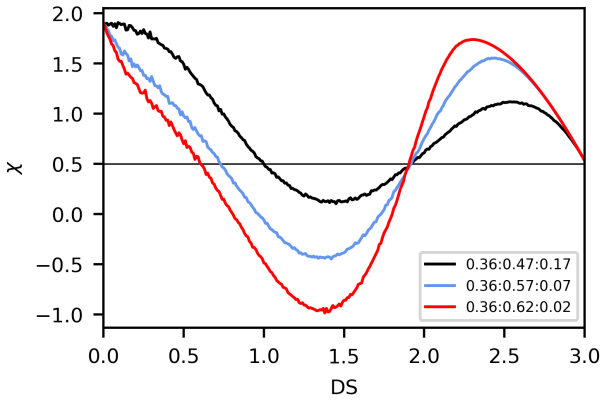

Figure 8: Effective χ of CA as a function of DS for sequences generated from three r_{set} values. The black series is from $r_{set} = 0.36 : 0.47 : 0.17$, same as Fig. 6A. The blue and red series are the results of modifying r_{set} by increasing the substitution rate at C3 while decreasing the substitution rate at C6. Their actual relative substituent compositions are shown in Fig. S10.

While Fig. 6 illustrates that the miscibility window occurs approximately between DS values of 1 and 2, which is higher than observed in experiments, it is important to note that Fig. 6 shows only an example slice of the phase diagram determined by the specific substituent composition shown in Fig. 5. Despite efforts to use NMR spectroscopy to analyze CA's substituent composition, accurately determining such composition in experiments remains challenging.[4,10,12,15,18] Therefore, it is not possible to match the experimental acetylation path and, consequently, the miscibility window. We demonstrate this point in Fig. 8, where the window is influenced by the relative composition of substituents at three alcohol sites. By increasing the substitution rate of C3 by 15% and correspondingly reducing it at C6 (by modifying r_{set} accordingly), the lower boundary of the miscibility window shifts to

0.6.

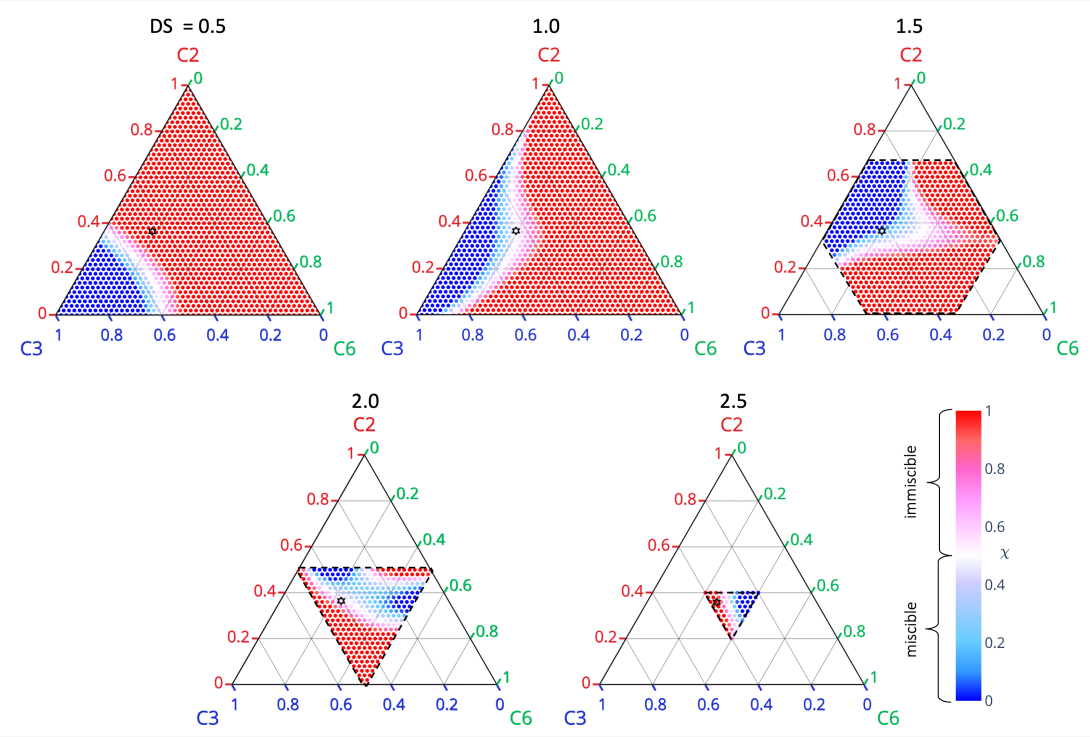

Figure 9: Miscibility assessed by the effective χ parameter in the acetylation composition space for DS = 0.5, 1.0, 1.5, 2.0, and 2.5. The χ value is represented by the color scale: blue ($\chi < 0.5$) denotes water-soluble CA while red ($\chi > 0.5$) corresponds to water-insoluble CA. The black star symbol denotes the substituent composition for the acetylation path in Fig. 6 at the corresponding DS. The black dashed line indicates the outer boundary of possible compositions at a given DS where applicable. See Fig. S11 for phase diagrams at additional DS values.

Using the developed model we further probe substituent compositions to develop design principles for engineering water-soluble CA. Specifically, at a fixed DS value, we calculate the effective χ for sequences spanning all possible substitution ratios of C2:C3:C6. Similar to previous calculations, we obtain the average χ over 1000 sequence generations at each relative acetylation ratio. As we have already established a strong correlation between effective χ values and miscibility, we use χ as a metric to assess miscibility: $\chi < 0.5$ corresponds to miscible samples while $\chi \geq 0.5$ corresponds to immiscible ones. Based on the results depicted in Fig. 9, which shows the miscibility of CA in the acetylation composition plane (r_{actual}), water-soluble CA is achieved when the majority of substitutions occur at C3 sites for low DS

values, around 0.5. From the relative orientation of the glucopyranose rings presented earlier, we hypothesize that substituting alcohol groups at the C3 site induces a conformational change sufficient to break apart the large hydrophobic plane at low substitution.[3,41]

At intermediate DS values, around 1.0-1.5, samples with substituents evenly distributed at C2 and C3 sites exhibit water solubility. This is consistent with the experimental study by Miyamoto et al. that lowering the relative substitution at C6 via altering the synthesis route results in water-soluble CA.[12] Finally, at high DS values, water-soluble CA are obtainable when the substituents are distributed relatively evenly among all three sites, with a slightly higher propensity for C2 and C6 sites. At these conditions, the orientation of glucopyranose rings along the backbone of CA have already undergone a significant conformational change and further acetylatation at the C3 sites becomes increasingly negligible; refer to Fig. S9. Instead, inter-molecular hydrogen bonding involving O2 and O6 becomes more crucial in maintaining the cohesion between cellulose chains. Consequently, substitutions at C2 and C6 sites become necessary to disrupt the cellulose network at higher DS values.

Notably, in recent work by Wu et al. on methylcellulose (MC) they also explain that at low to moderate DS values (<1.2) the hydrogen bonding network of cellulose is disrupted with the remaining unsubstituted -OH groups better available for water to hydrogen bond with than in native cellulose.[47] They also point out that the observed nonmonoticity of MC's solubility in water is due to the competing effects of increased cellose-water hydrogen bonding at intermediate substitution before hydrophobic interactions dominate at higher DS values. Broadly speaking, based on our modeling results and those of Wu et al., it appears that both CA and MC solubility in water experience the same driving forces.

Lastly, one inconsistency we observe in the current model is that CA becomes miscible at DS=3, indicated by the disappearance of the two-phase region. In fact, DS=3 is right on the cusp of immisicibility with a $\chi \sim 0.5$ (see Fig. 6A). Importantly, we also observe this weakening of immiscibility with increasing acetylation in the AA simulations, as evidenced by the decrease in the peak intensity of the radial distribution function (RDF) between

inter-molecular glucose units as DS approaches 3 (Fig. S12A). Thus, CA also becomes more hydrated at DS=3 in the AA simulations. The fact that the CG model correctly captures the AA model's solution phase behavior at DS=3 indicates that the model performs well in this regard. Nevertheless, the discrepancy with experimental findings is likely attributable to the crystallization of cellulose triacetate, a phenomenon not captured in AAMD due to the long timescales and the relatively small molecular weight of the CA used in our study. Consequently, the model inadequately considers the free energy gain from crystallization, which can drive phase separation at both high and low DS values.[48–50] We acknowledge that solid-liquid equilibrium is likely more important in these limits, but leave this direction to future work.

Our focus in this work is on addressing CA miscibility within the intermediate DS range, which is more relevant in formulation design and where the random placement of acetate moieties along the chain backbone is expected to promote amorphous CA. Indeed, we observe that the CG model captures the decreasing peak intensity of the mapped AA sites in the interchain RDFs, a signature of the weakening aggregation of the CA chains in water as DS increases (Fig. S12A). Likewise, the CG model also captures the corresponding increasing number of water molecules around the CG sites observable in the mapped AA model $G_x - w$ RDFs, Fig. S12B. Moreover, these results give an indication that the CG model is indeed faithful to the underlying AA reference system and would suggest discrepancies between experiment and the CG model stem from inaccuracies in the AA model itself. However, detailed investigations are required to precisely identify the origin of errors along with precise experimental data to compare against.

4 Conclusions

In this study, we developed a molecularly informed field-theoretic model for cellulose acetate (CA), an important ester derivative of cellulose, and investigated its phase behavior in

aqueous solutions. Our coarse-grained (CG) model represents CA with 8 monomer types, categorized by the degree-of-substitution (DS) and the specific acetylation sites. Particularly, the model predicts a miscibility window at intermediate DS values (approximately 0.6-2), which qualitatively aligns with experimental findings. This is especially remarkable since we are able to capture the nontrivial phase behavior, where CA solutions transition from insoluble to soluble and back to insoluble. While experimental studies have a wide range of DS values over which CA is water-soluble, we are able to use a molecularly informed field theory to directly probe CA solution behavior as a function of the relative DS at the three alcohol sites, C2, C3, and C6. Specifically, our results suggest the optimal relative substituent ratios at these different sites for water-soluble CA depend on the overall DS.

For future work we see two exciting opportunities. The first is, as discussed above, to include crystallization thermodynamics into the calculations, which is particularly important for polymers that have no sequence homogeneity that serves to disrupt lattice packing. If the free energy of fusion is known for the neat polymer, the polymer activity in a given solvent can be computed using the CG model; then the polymer solubility can be computed directly as done in solid-liquid equilibria calculations.[51] The second direction is charting out the cellulose solubility as a function of temperature. The most straight-forward approach would involve repeating the workflow at different temperatures over the range of interest and interpolating during the phase coexistenece calculations.[20]

In general, our multiscale workflow enables the correlation of atomic level interactions (hydrogen bonding and glucopyranose ring conformational changes) with macroscopic CA miscibility as a function of DS. Regardless of the underlying mechanisms, charting the miscibility window as a function of DS enables the rational design of water-soluble CA with tailored properties for a wide-range of applications. While in this work we have focused solely on cellulose and its acetate derivative, this methodology is generally applicable to other carbohydrates and their derivatives in a wide variety of solvents as long as there exists a suitable atomistic forcefield and the polymer(s) are not too stiff (i.e., large persistence

lengths) or exhibit secondary structures. We believe there is great promise in coupling this level of modeling with wet-lab experimentation to aid in the engineering of next-generation polymeric materials with tailored properties, such as solubility.

Supporting Information Available

Details for all-atom simulations, force field parameters of the coarse-grained model, conformational analysis and additional phase diagrams are available in the Supporting Information.

Acknowledgement

This work was supported by BASF Corporation and BASF SE through the California Research Alliance. G.H.F. acknowledges support from the National Science Foundation CMMT Program under Grant No. DMR-2104255. M.S.S. acknowledges funding support from the National Science Foundation through Award No. CHEM-1800344. Use was made of the BioPACIFIC Materials Innovation Platform computing resources of the National Science Foundation Award No. DMR-1933487 and computational facilities purchased with funds from the National Science Foundation (CNS-1725797) and administered by the Center for Scientific Computing (CSC). The CSC is supported by the California NanoSystems Institute and the Materials Research Science and Engineering Center (MRSEC; NSF DMR-2308708) at UC Santa Barbara.

References

(1) Klemm, D.; Heublein, B.; Fink, H.-P.; Bohn, A. Cellulose: fascinating biopolymer and sustainable raw material. *Angewandte chemie international edition* **2005**, *44*, 3358–3393.

(2) Wu, Z.; Beltran-Villegas, D. J.; Jayaraman, A. Development of a New Coarse-Grained Model to Simulate Assembly of Cellulose Chains Due to Hydrogen Bonding. *16*, 4599–4614, DOI: 10.1021/acs.jctc.0c00225, Publisher: American Chemical Society.

(3) Medronho, B.; Romano, A.; Miguel, M. G.; Stigsson, L.; Lindman, B. Rationalizing cellulose (in)solubility: reviewing basic physicochemical aspects and role of hydrophobic interactions. *19*, 581–587, DOI: 10.1007/s10570-011-9644-6.

(4) Pang, J.; Liu, X.; Yang, J.; Lu, F.; Wang, B.; Xu, F.; Ma, M.; Zhang, X. Synthesis of highly polymerized water-soluble cellulose acetate by the side reaction in carboxylate ionic liquid 1-ethyl-3-methylimidazolium acetate. *Scientific reports* **2016**, *6*, 33725.

(5) Kostag, M.; Gericke, M.; Heinze, T.; El Seoud, O. A. Twenty-five years of cellulose chemistry: innovations in the dissolution of the biopolymer and its transformation into esters and ethers. *26*, 139–184, DOI: 10.1007/s10570-018-2198-0.

(6) Deus, C.; Friebolin, H.; Siefert, E. Partiell acetylierte cellulose—synthese und bestimmung der substituentenverteilung mit hilfe der 1H NMR-spektroskopie. *Die Makromolekulare Chemie: Macromolecular Chemistry and Physics* **1991**, *192*, 75–83.

(7) Samios, E.; Dart, R.; Dawkins, J. Preparation, characterization and biodegradation studies on cellulose acetates with varying degrees of substitution. *38*, 3045–3054, DOI: 10.1016/S0032-3861(96)00868-3.

(8) Yadav, N.; Hakkarainen, M. Degradable or not? Cellulose acetate as a model for complicated interplay between structure, environment and degradation. *Chemosphere* **2021**, *265*, 128731, DOI: 10.1016/j.chemosphere.2020.128731.

(9) Heinze, T.; Liebert, T. Celluloses and polyoses/hemicelluloses. **2012**,

(10) Kamide, K.; Okajima, K.; Kowsaka, K.; Matsui, T. Solubility of cellulose acetate pre-

pared by different methods and its correlationships with average acetyl group distribution on glucopyranose units. *Polymer journal* **1987**, *19*, 1405–1412.

(11) Steinmeier, H. 3. Acetate manufacturing, process and technology 3.1 Chemistry of cellulose acetylation. *208*, 49–60, DOI: 10.1002/masy.200450405, Publisher: John Wiley & Sons, Ltd.

(12) Miyamoto, T.; Sato, Y.; Shibata, T.; Tanahashi, M.; Inagaki, H. 13C-NMR spectral studies on the distribution of substituents in water-soluble cellulose acetate. *Journal of Polymer Science: Polymer Chemistry Edition* **1985**, *23*, 1373–1381.

(13) Tian, D.; Han, Y.; Lu, C.; Zhang, X.; Yuan, G. Acidic ionic liquid as "quasi-homogeneous" catalyst for controllable synthesis of cellulose acetate. *Carbohydrate polymers* **2014**, *113*, 83–90.

(14) Gomez-Bujedo, S.; Fleury, E.; Vignon, M. R. Preparation of cellouronic acids and partially acetylated cellouronic acids by TEMPO/NaClO oxidation of water-soluble cellulose acetate. *Biomacromolecules* **2004**, *5*, 565–571.

(15) Wolfs, J.; Meier, M. A. A more sustainable synthesis approach for cellulose acetate using the DBU/CO 2 switchable solvent system. *Green Chemistry* **2021**, *23*, 4410–4420.

(16) Kamide, K.; Saito, M.; Abe, T. Dilute solution properties of water-soluble incompletely substituted cellulose acetate. *Polymer Journal* **1981**, *13*, 421–431.

(17) Crane, C. L. Method of preparing far-hydrolyzed cellulose esters. 1943; US Patent 2,327,770.

(18) Buchanan, C. M.; Edgar, K. J.; Wilson, A. K. Preparation and characterization of cellulose monoacetates: the relationship between structure and water solubility. *Macromolecules* **1991**, *24*, 3060–3064.

(19) Shen, K.; Sherck, N.; Nguyen, M.; Yoo, B.; Köhler, S.; Speros, J.; Delaney, K. T.; Fredrickson, G. H.; Shell, M. S. Learning composition-transferable coarse-grained models: Designing external potential ensembles to maximize thermodynamic information. *The Journal of Chemical Physics* **2020**, *153*, 154116.

(20) Sherck, N.; Shen, K.; Nguyen, M.; Yoo, B.; Kohler, S.; Speros, J. C.; Delaney, K. T.; Shell, M. S.; Fredrickson, G. H. Molecularly Informed Field Theories from Bottom-up Coarse-Graining. *ACS Macro Letters* **2021**, *10*, 576–583.

(21) Nguyen, M.; Sherck, N.; Shen, K.; Edwards, C. E.; Yoo, B.; Köhler, S.; Speros, J. C.; Helgeson, M. E.; Delaney, K. T.; Shell, M. S.; Fredrickson, G. H. Predicting Polyelectrolyte Coacervation from a Molecularly Informed Field-Theoretic Model. *Macromolecules* **2022**,

(22) Nguyen, M. V.; Dolph, K.; Delaney, K. T.; Shen, K.; Sherck, N.; Köhler, S.; Gupta, R.; Francis, M. B.; Shell, M. S.; Fredrickson, G. H. Molecularly informed field theory for estimating critical micelle concentrations of intrinsically disordered protein surfactants. *The Journal of Chemical Physics* **2023**, *159*.

(23) Nguyen, M.; Shen, K.; Sherck, N.; Köhler, S.; Gupta, R.; Delaney, K. T.; Shell, M. S.; Fredrickson, G. H. A molecularly informed field-theoretic study of the complexation of polycation PDADMA with mixed micelles of sodium dodecyl sulfate and ethoxylated surfactants. *The European Physical Journal E* **2023**, *46*, 75.

(24) Guvench, O.; Mallajosyula, S. S.; Raman, E. P.; Hatcher, E.; Vanommeslaeghe, K.; Foster, T. J.; Jamison, F. W.; MacKerell Jr, A. D. CHARMM additive all-atom force field for carbohydrate derivatives and its utility in polysaccharide and carbohydrate–protein modeling. *Journal of chemical theory and computation* **2011**, *7*, 3162–3180.

(25) Izadi, S.; Anandakrishnan, R.; Onufriev, A. V. Building water models: a different approach. *J. Phys. Chem. Lett.* **2014**, *5*, 3863–3871.

(26) Eastman, P.; Swails, J.; Chodera, J. D.; McGibbon, R. T.; Zhao, Y.; Beauchamp, K. A.; Wang, L.-P.; Simmonett, A. C.; Harrigan, M. P.; Stern, C. D.; others OpenMM 7: Rapid development of high performance algorithms for molecular dynamics. *PLoS computational biology* **2017**, *13*, e1005659.

(27) Humphrey, W.; Dalke, A.; Schulten, K. VMD: visual molecular dynamics. *Journal of molecular graphics* **1996**, *14*, 33–38.

(28) Martínez, L.; Andrade, R.; Birgin, E. G.; Martínez, J. M. PACKMOL: A package for building initial configurations for molecular dynamics simulations. *Journal of computational chemistry* **2009**, *30*, 2157–2164.

(29) Shen, K.; Nguyen, M.; Sherck, N.; Yoo, B.; Köhler, S.; Speros, J.; Delaney, K. T.; Shell, M. S.; Fredrickson, G. H. Predicting Surfactant Phase Behavior with a Molecularly Informed Field Theory. *Journal of Colloid and Interface Science* **2023**,

(30) Shell, M. S. Coarse-graining with the relative entropy. *Advances in chemical physics* **2016**, *161*, 395–441.

(31) Fredrickson, G. H.; Delaney, K. T. *Field-Theoretic Simulations in Soft Matter and Quantum Fluids*; Oxford University Press, 2023; Vol. 173.

(32) MacQueen, J.; others Some methods for classification and analysis of multivariate observations. Proceedings of the fifth Berkeley symposium on mathematical statistics and probability. 1967; pp 281–297.

(33) Lloyd, S. Least squares quantization in PCM. *IEEE transactions on information theory* **1982**, *28*, 129–137.

(34) Forgy, E. W. Cluster analysis of multivariate data: efficiency versus interpretability of classifications. *biometrics* **1965**, *21*, 768–769.

(35) Pedregosa, F. et al. Scikit-learn: Machine Learning in Python. *Journal of Machine Learning Research* **2011**, *12*, 2825–2830.

(36) Edwards, S. F. The statistical mechanics of polymers with excluded volume. *Proceedings of the Physical Society* **1965**, *85*, 613.

(37) Fredrickson, G.; others *The equilibrium theory of inhomogeneous polymers*; Oxford University Press on Demand, 2006; Vol. 134.

(38) Flory, P. J. Thermodynamics of high polymer solutions. *The Journal of chemical physics* **1941**, *9*, 660–660.

(39) Huggins, M. L. Solutions of long chain compounds. *The Journal of chemical physics* **1941**, *9*, 440–440.

(40) De Gennes, P.-G.; Gennes, P.-G. *Scaling concepts in polymer physics*; Cornell university press, 1979.

(41) Lindman, B.; Karlström, G.; Stigsson, L. On the mechanism of dissolution of cellulose. *156*, 76–81, DOI: 10.1016/j.molliq.2010.04.016.

(42) Parthasarathi, R.; Bellesia, G.; Chundawat, S. P. S.; Dale, B. E.; Langan, P.; Gnanakaran, S. Insights into Hydrogen Bonding and Stacking Interactions in Cellulose. *115*, 14191–14202, DOI: 10.1021/jp203620x, Publisher: American Chemical Society.

(43) McNamara, J. T.; Morgan, J. L.; Zimmer, J. A Molecular Description of Cellulose Biosynthesis. *84*, 895–921, DOI: 10.1146/annurev-biochem-060614-033930.

(44) Bergenstråhle-Wohlert, M.; Angles d'Ortoli, T.; Sjöberg, N. A.; Widmalm, G.; Wohlert, J. On the anomalous temperature dependence of cellulose aqueous solubility. *23*, 2375–2387, DOI: 10.1007/s10570-016-0991-1.

(45) Wohlert, M.; Benselfelt, T.; Wågberg, L.; Furó, I.; Berglund, L. A.; Wohlert, J. Cellulose and the role of hydrogen bonds: not in charge of everything. *29*, 1–23, DOI: 10.1007/s10570-021-04325-4.

(46) Nishiyama, Y. Molecular interactions in nanocellulose assembly. *376*, 20170047, DOI: 10.1098/rsta.2017.0047.

(47) Wu, Z.; Collins, A. M.; Jayaraman, A. Understanding Self-Assembly and Molecular Packing in Methylcellulose Aqueous Solutions Using Multiscale Modeling and Simulations. *Biomacromolecules* **2024**, *25*, 1682–1695, DOI: 10.1021/acs.biomac.3c01209, Publisher: American Chemical Society.

(48) Kamide, K.; Saito, M. Thermal Analysis of Cellulose Acetate Solids with Total Degrees of Substitution of 0.49, 1.75, 2.46, and 2.92. *17*, 919–928, DOI: 10.1295/polymj.17.919.

(49) Dale, B. E.; Tsao, G. T. Crystallinity and heats of crystallization of cellulose: A microcalorimetric investigation. *27*, 1233–1241, DOI: 10.1002/app.1982.070270412, Publisher: John Wiley & Sons, Ltd.

(50) Barud, H. S.; de Araújo Júnior, A. M.; Santos, D. B.; de Assunção, R. M.; Meireles, C. S.; Cerqueira, D. A.; Rodrigues Filho, G.; Ribeiro, C. A.; Messaddeq, Y.; Ribeiro, S. J. Thermal behavior of cellulose acetate produced from homogeneous acetylation of bacterial cellulose. *471*, 61–69, DOI: 10.1016/j.tca.2008.02.009.

(51) Gmehling, J.; Kleiber, M.; Kolbe, B.; Rarey, J. *Chemical thermodynamics for process simulation*, second, completely revised and enlarged edition ed.; Wiley-VCH.